Volume 13
Number 47
21 December 2025
Pages 40377–41404

Journal of Materials Chemistry A

Materials for energy and sustainability

rsc.li/materials-a

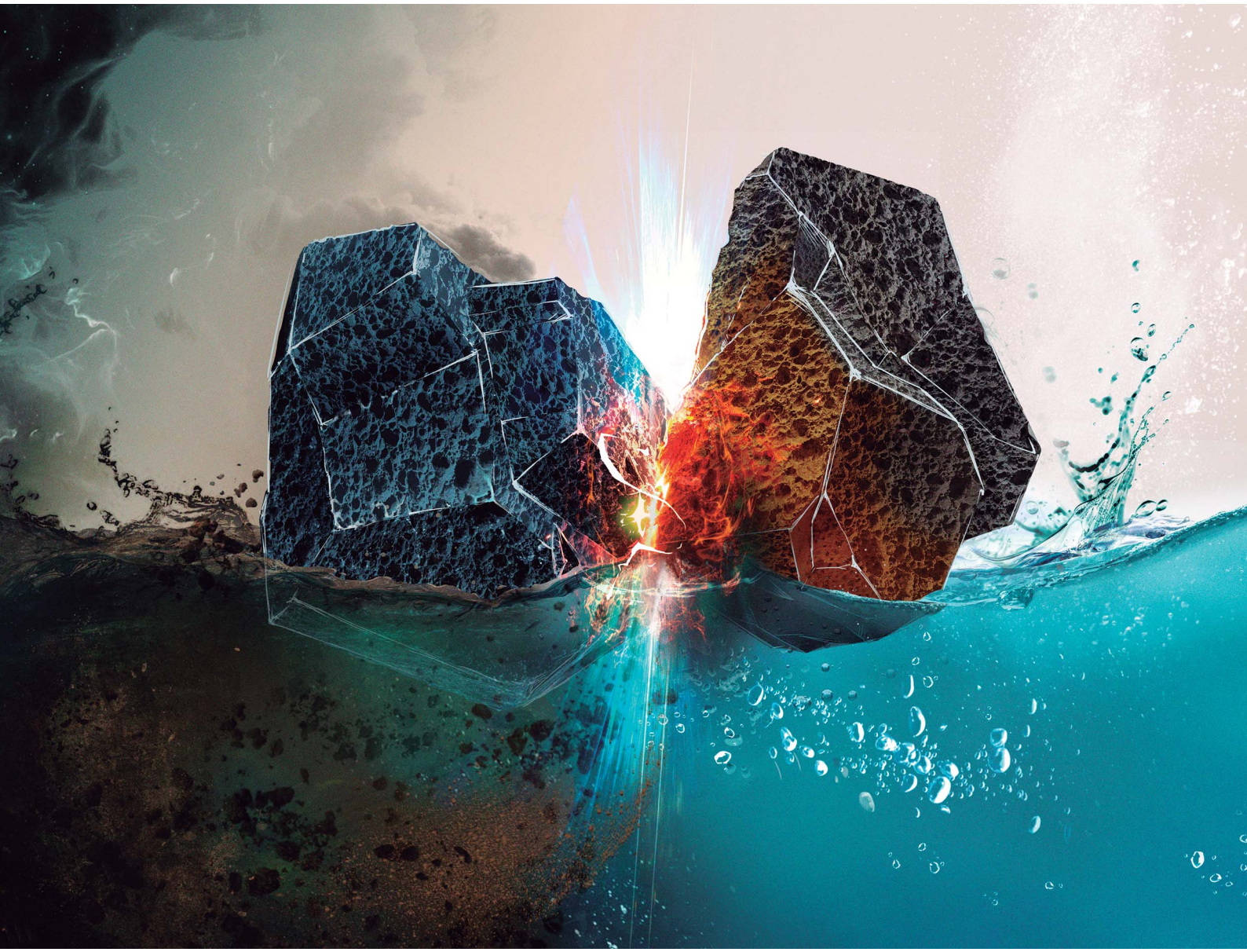

ISSN 2050-7488

ROYAL SOCIETY OF CHEMISTRY

PAPER

Félix Zamora, Carmen Montoro, Ana E. Platero-Prats *et al.*
Deciphering interfacial interactions in a dual-functional MOF@COF composite for organic pollutant removal from water

Journal of Materials Chemistry A

ROYAL SOCIETY OF CHEMISTRY

PAPER

View Article Online
View Journal | View Issue

Check for updates

Cite this: *J. Mater. Chem. A*, 2025, **13**, 40665

Deciphering interfacial interactions in a dual-functional MOF@COF composite for organic pollutant removal from water

Isabel del Castillo-Velilla, [a] Celia Castillo-Blas, [b] Thomas D. Bennett, [bc] Beatriz Cuadrado-Benavent,[a] Félix Zamora, [*ad] Carmen Montoro [*ae] and Ana E. Platero-Prats [*ad]

Received 25th April 2025
Accepted 9th August 2025

DOI: 10.1039/d5ta03279b

rsc.li/materials-a

MOF@COF composites have emerged as a promising class of engineered materials with unique functionalities, combining the high porosity and tunability of metal–organic frameworks (MOFs) with the chemical and mechanical stability of covalent-organic frameworks (COFs). While their advantageous properties are well-recognized, their structural intricacies and the nature of the interfacial interactions remain insufficiently explored. In this study, an Fe-MOF@COF composite is presented, exhibiting dual functionalities for the efficient removal of organic pollutants from water. The enhanced performance is attributed to the unique properties of the MOF–COF interface, where synergistic interactions between the two porous materials play a critical role. Advanced synchrotron techniques were employed to probe interfacial interactions at the atomic and molecular levels. These findings underscore the potential of Fe-MOF@COF composites as highly effective materials for water remediation, providing deeper insights into their structural behavior and interfacial properties.

Ana E. Platero-Prats

Ana E. Platero-Prats is a group leader at the Universidad Autónoma de Madrid (UAM), where she develops hybrid porous materials—particularly metal–organic frameworks (MOFs) and covalent-organic frameworks (COFs)—for environmental remediation, water treatment, and catalysis. Fascinated by their atomic structure, she uses synchrotron-based techniques, such as Pair Distribution Function (PDF) analysis, to link structural details with material performance. She earned her PhD at the ICMM-CSIC, with research stays at the Institute Lavoisier de Versailles and the Università degli Studi di Milano, and held postdoctoral positions at Stockholm University and Argonne National Laboratory. Outside the lab, she is a mother of two girls, mastering time management as an exact science.

Introduction

Metal–organic frameworks (MOFs) and covalent organic frameworks (COFs) are typically crystalline porous materials that have revolutionized reticular chemistry in recent years. The main distinction between them lies in their composition: MOFs consist of metal nodes coordinated to organic ligands, whereas COFs are made entirely of organic monomers linked by covalent bonds.[1,2] They both present interesting properties such as high porosity, associated with excellent sorption capacities, thermal and chemical stability, chemical tailorability, and stabilization of active sites. Consequently, they are recognized for their wide range of applications across various fields such as drug delivery,[3] water remediation,[4,5] or gas adsorption and separation.[6] However, despite these promising characteristics, their industrial implementation is still challenging, as they are often obtained in the form of microcrystalline powders, which makes them difficult to handle, scale up, and integrate into processes.[7,8]

[a]*Departamento de Química Inorgánica, Facultad de Ciencias, Universidad Autónoma de Madrid, Campus de Cantoblanco, Madrid, 28049, Spain. E-mail: felix.zamora@uam.es; carmen.montoro@uam.es; ana.platero@uam.es*

[b]*Department of Materials Science and Metallurgy, University of Cambridge, Cambridge CB3 0FS, UK*

[c]*School of Physical and Chemical Sciences, University of Canterbury, Christchurch 8140, New Zealand*

[d]*Condensed Matter Physics Center (IFIMAC), Universidad Autónoma de Madrid, Campus de Cantoblanco, Madrid, 28049, Spain*

[e]*Institute for Advanced Research in Chemical Sciences (IAdChem), Universidad Autónoma de Madrid, Campus de Cantoblanco, Madrid, 28049, Spain*

In this context, composites combining MOFs and COFs have recently been developed, offering promising potential due to their enhanced properties and significant advantages in terms of processability and multifunctionality.[9,10] These materials can be obtained through various approaches, either by combining pre-synthesized COF and MOF components or by integrating one material into the synthesis process of the other. In terms of the assembly of the hybrid composites, this can be driven by different interactions: coordination or covalent bonds, hydrogen bonding, or π–π stacking interactions between the COF and MOF components.[11] These factors, along with the type and size of the COF and MOF and their pore sizes, determine the structure of the composite, leading to two primary variations: core–shell structures and heterostructures.[12–15] The interfacial interactions within these composites are crucial as they determine the mechanical stability and the emergence of novel dual properties that distinguish these composites from a simple physical mixture.[16] Nevertheless, characterizing these interfacial interactions in MOF@COF composites remains a major challenge due to their nature and trace proportion compared to the bulk, requiring detailed and rigorous analysis.

In pursuit of developing a stable hybrid composite with dual functionality for the capture and degradation of water pollutants, we prepared a heterostructured MOF@COF combining MOF-808 and TAPB–BTCA-COF. MOF-808 consists of Zr_6O_8 metal clusters connected to benzene-1,3,5-tricarboxylate linkers (BTC, $C_9H_3O_6$), with the general formula $[Zr_6O_8H_4(C_9H_3O_6)_2(HCO_2)_6]$, synthesized using formic acid as the modulator (Fig. 1A).[17] Functionalization of MOF-808 with transition metals can enhance its catalytic properties, such as in the Fenton reaction through iron incorporation.[18,19] Meanwhile, TAPB–BTCA-COF, formed from 1,3,5-tris(4-aminophenyl)benzene (TAPB) and 1,3,5-benzenetricarbaldehyde (BTCA), assembled into a two-dimensional ($C_{33}H_{21}N_3$) lattice (Fig. 1B).[20] This water-stable, imine-based COF shows high adsorption capacity for bisphenol A (BPA) and provides superior mechanical stability, improving processability.[21,22]

In this work, we present the development of a MOF@COF composite specifically designed for water remediation. A detailed structural investigation was conducted using a recently reported analysis methodology based on the pair distribution function (PDF) to gain critical insights into the local structure and the nature of interfacial interactions. The findings from PDF analysis were further corroborated by diffuse reflectance spectroscopy (DRS) and vapour adsorption isotherms. This advanced characterisation revealed a well-defined interface within the composite, which imparts a unique dual functionality, making it highly effective for the simultaneous capture and degradation of water contaminants under continuous flow conditions.

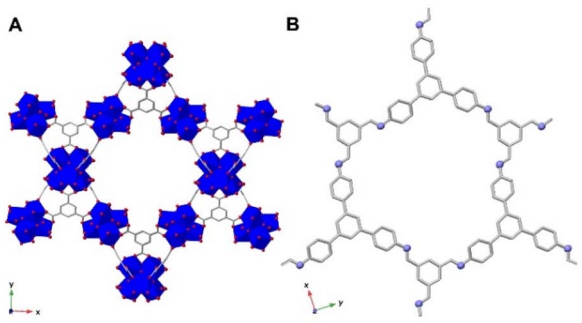

Fig. 1 Representation of the (A) MOF-808 structure and (B) TAPB–BTCA-COF structure. Colour scheme: blue = Zr, grey = C, red = O, lilac = N; hydrogen atoms have been omitted for clarity.

Results and discussion

Composite synthesis and characterisation

MOF-808 was synthesized as nanoparticles in gel form (see S1 from SI), to avoid aggregation and achieve a homogeneous dispersion of the MOF within the COF matrix (see S2 from SI).[23] Subsequently, the MOF-808 gel was metalated with iron by immersion in a methanol solution containing iron(II) acetate ($Fe(CH_3COO)_2$) at 60 °C overnight, yielding Fe-MOF-808 (see S1 from SI). Chemical analyses indicated a Fe to Zr_6O_8 molar ratio of approximately 4.0.

The hybrid composite was prepared by dispersing the Fe-MOF-808 gel in an aqueous acetic acid solution with the COF precursors, allowing the composite to form concurrently with the COF in a one-step synthetic approach *via* a sonochemical reaction using an ultrasound transducer for 1 h.[24,25] This work aimed to incorporate the highest possible amount of MOF—identified as the catalytically active phase—while preserving the homogeneity of the composite. A MOF loading of 7 mol% was found to be optimal; higher contents led to phase separation, as demonstrated by SEM-EDS analysis (see Table S1.1). Consequently, lower MOF loadings were not investigated in detail. Chemical analyses revealed partial leaching of iron cations, likely due to the slightly acidic medium and strong sonication conditions, resulting in a final Fe to Zr_6O_8 molar ratio of 1.8. For comparison, we also worked with a physical mixture of Fe-MOF-808 and TAPB–BTCA-COF, prepared with the same ratio of components as in the composite.

Powder X-ray diffraction (PXRD) data for the composite exhibited Bragg peaks corresponding to the TAPB–BTCA-COF phase, with minor contributions from the MOF phase (see Fig. S3.3 from SI). Fourier transform infrared spectroscopy (FTIR) confirmed the presence of characteristic vibrational bands of the MOF-808 and TAPB–BTCA-COF (see Fig. S4.3 from SI). Proton nuclear magnetic resonance (^{1}H NMR) of digested MOF gel samples, along with elemental analysis, enabled the determination of the chemical formula for the Fe-MOF@COF composite as $[Zr_6Fe_{1.8}O_8H_4(C_9H_3O_6)_2(COOH)_1(OH)_{8.4}(H_2O)_5(C_2H_3O_2)_2]_{0.07}$ + $[C_{33}H_{21}N_3]_{0.93}$ (see S1 and S5 from SI). Transmission electron microscopy (TEM) revealed the formation of aggregates in the composite (Fig. 2A and S6 from SI). Field emission scanning electron microscopy (FE-SEM) with energy dispersive X-ray spectroscopy (EDX) showed by linear mapping analysis the uniform incorporation of Fe-MOF-808 within the composite (Fig. 2B and C), with no evidence of domain formation observed. Thermal gravimetric analyses (TGA) indicated

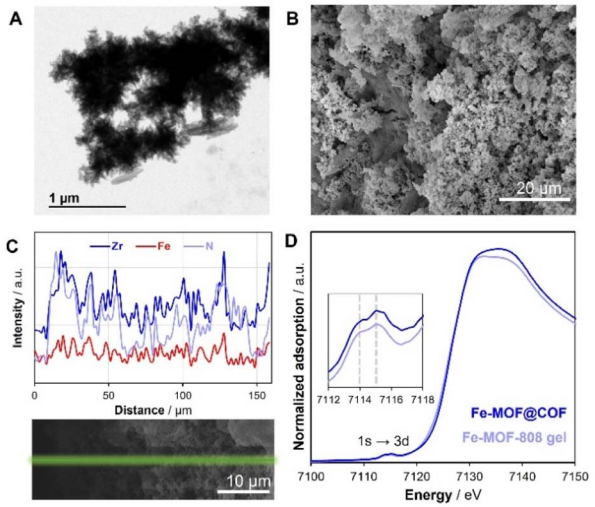

Fig. 2 (A) TEM image of Fe-MOF@COF. (B) FE-SEM image of Fe-MOF@COF. (C) FE-SEM-EDX line scan of the cross-sectional area of Fe-MOF@COF. (D) Fe K-edge XANES for the Fe-MOF-808 gel and Fe-MOF@COF.

thermal stability of the hybrid composite up to approximately 300 °C (see S8 from SI).

The local structure of the composite was investigated using advanced synchrotron characterisation techniques. X-ray absorption spectroscopy (XAS) experiments were performed to elucidate the geometry and oxidation state of iron in the composite. Fe K-edge data from X-ray absorption near edge structure (XANES) for the Fe-MOF-808 gel and Fe-MOF@COF at 150 K showed two pre-edge peaks at 7114 and 7115 eV, indicating an octahedral binuclear geometry of iron(III) sites in both materials (Fig. 2D).[26] Meanwhile, Fe K-edge data from extended X-ray absorption fine structure (EXAFS) revealed a main peak at 2.0 Å (after phase correction) corresponding to Fe(III)–O bonds and two additional peaks at 2.9 Å and 3.4 Å (after phase correction) corresponding to Fe(III)···M distances (see Fig. S9.1 from SI). These results confirm the stabilization of Fe(III)–oxo sites within MOF-808.

To verify the formation of a true MOF@COF composite, rather than two separate materials, the textural properties of the composite were investigated through nitrogen adsorption isotherms measured at 77 K (see S10 from SI).[27] The results revealed distinct porosity differences between the composite and the physical mixture, suggesting the presence of an interface. The composite exhibited a steeper nitrogen uptake at low relative pressures, indicative of dominant microporosity, while the physical mixture exhibits a more gradual characteristic of mesoporous features (see Fig. S10.1 and S10.8 from SI). Further surface area analysis demonstrated that the composite has a significantly higher micropore area and a lower external surface area compared to the physical mixture (see Table S10.1 from SI). Additionally, NLDFT pore size distribution analysis revealed a greater contribution of micropores in the composite compared to the physical mixture, as well as differences in mesopore distribution (see Fig. S10.8 from SI).

Structural characterisation of the interface

To gain further insights into the structural characteristics of the composite interface, advanced techniques were employed to analyse its molecular architecture. PDF analysis of X-ray total scattering data is a versatile characterisation technique for determining atom–atom distances, regardless of crystallinity, making it a valuable tool for tackling challenges in materials science, particularly in the characterisation of MOFs and COFs.[28,29] Using differential analysis of the PDF (dPDF) data (obtained by subtracting PDFs of the MOF-808 gel from the Fe-MOF-808 gel), we were able to study the atomic structure of the iron sites within the MOF-808 gel structure (see Fig. S11.1 from SI), with results that aligned closely with the findings from EXAFS (see Fig. S9.1 from SI). Then, to examine the retention of the MOF structure, the PDF profile of the COF was subtracted from the total PDF profile of Fe-MOF@COF, revealing peaks at 2.2 Å (Zr–O bonds), 3.5 Å and 5.0 Å (Zr···Zr distances) characteristic of Zr_6O_8 clusters in MOF-808 (see Fig. S11.2A from SI). Conversely, for the COF structure, the expected distances at 1.5 Å (C=C bonds), 2.5 Å (C···C bonds), and 3.8–5.0 Å (π–π stacking) were observed (see Fig. S11.2B from SI).

To further explore the nature of this interface between the MOF and COF, an extended study was conducted using PDF data, in combination with multiple linear regression (MLR) analysis. MLR is a statistical modelling used to estimate the relationships between two or more variables. These variables are classified as the dependent variable, which represents the main factor being studied and predicted, and the independent variables, which are the factors that might influence the dependent one. MLR can determine how two or more independent variables can predict the outcome of a dependent variable, following in this case, the equation: $G(r)_{\text{composite}} = A \times G(r)_{\text{COF}} + B \times G(r)_{\text{Fe-MOF}} + C$, where C is a normalization constant.[30,31] From it, we can then predict the ideal PDF pattern of the dependent variable (the composite) based on component data from the COF and Fe-MOF. Furthermore, a residual pattern is obtained from the differences between the experimental and calculated data, which offers insights into potential interactions within the system (Fig. 3). To ensure accuracy, we compared the residual patterns of the hybrid composite and the physical mixture. This analysis revealed the presence of a new broad contribution centred at 3.1 Å, along with variations in the intensity of signals at 2.5 and 2.7 Å, highlighting the true characteristics of the interface. This distance suggests the presence of new strong π–π stacking interactions between the MOF organic backbone and COF monomers (Fig. 3) as well as hydrogen bonding. These findings were further confirmed using principal component analysis (PCA) of the PDF data (see Fig. S11.5 from SI).

DRS analysis was conducted to investigate the presence of π–π stacking interactions. The resulting data revealed a 10 nm redshift in the composite spectrum compared to both the physical mixture and the COF reference (Fig. 4). This observed redshift provides evidence of new π–π stacking interactions. To confirm that this shift was not solely due to the intrinsic π–π stacking interactions within the COF component, the materials

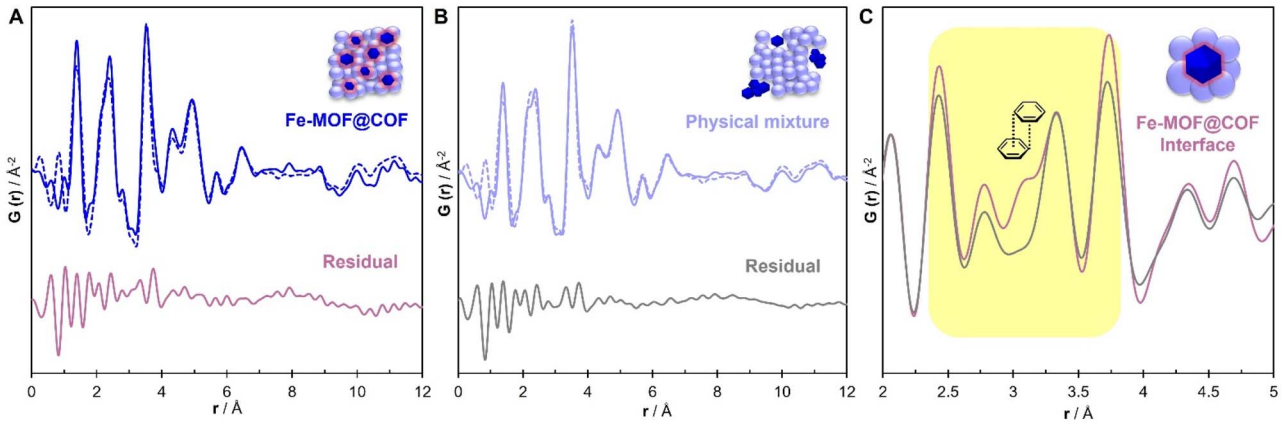

Fig. 3 MLR analysis of PDF data. (A) MLR analysis on Fe-MOF@COF composite data. (B) MLR analysis on the physical mixture data. The experimental patterns for Fe-MOF@COF and the physical mixture are shown as solid lines and the ideal patterns are shown as dashed lines. (C) Comparison between the residual patterns for the composite and for the physical mixture, emphasizing the nature of the interface.

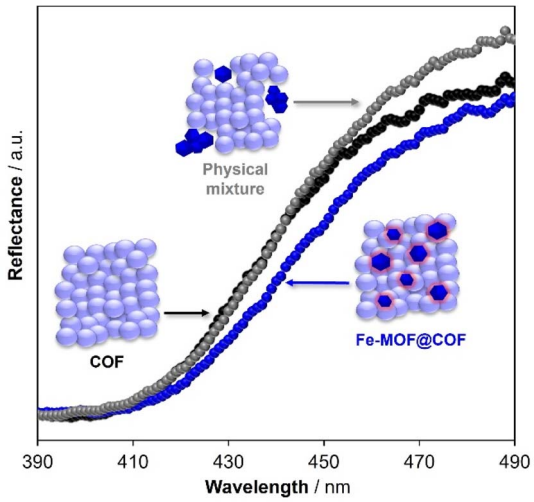

Fig. 4 Diffuse reflectance spectroscopy data of the physical mixture, the COF, and the Fe-MOF@COF composite.

were treated with a NaOH solution (pH 12) to decompose the Fe-MOF-808 in both the physical mixture and the composite (see Fig. S12.1 from SI). As anticipated, the redshift was no longer observed in the composite, indicating that the π–π stacking interactions occur specifically between the MOF ligands and the COF monomers.[32] Additionally, the band gaps of the materials were calculated from Kubelka–Munk-transformed spectra showing the same tendency (see Fig. S12.2 from SI). These results confirm that the electronic structure of the composite is directly influenced by MOF-COF interactions, highlighting their role in enhancing the material's performance for water remediation.

Porosity of the interface

To validate the porosity of the interface toward organic molecules relevant to water treatment, a series of experiments were conducted to evaluate adsorption capacity and molecular accessibility. Benzene adsorption isotherms were performed as a benchmark test to probe the accessibility of aromatic molecules capable of establishing π–π stacking interactions with the composite interface. The results revealed that both the composite material and the physical mixture exhibit a type II sorption curve. However, Fe-MOF@COF demonstrated a significantly higher benzene adsorption capacity compared to the physical mixture (Fig. 5). This enhancement may be attributed to the presence of a thicker interface, which is a consequence of the synergistic interactions between the two components of the composite. The aromatic surface created by this synergy facilitates π–π stacking interactions and enhances molecular accessibility. Additionally, the adsorption of other vapors, such as water and ethanol, was investigated to provide further insight and rule out potential alternative interactions, such as hydrogen bonding (see Fig. S13.1 from SI). These findings revealed the

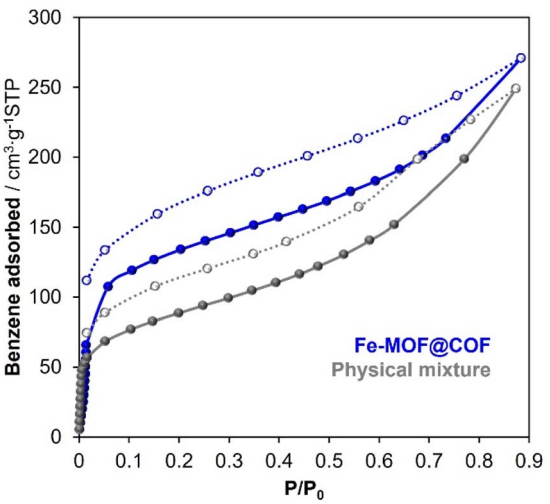

Fig. 5 Benzene adsorption (solid line) and desorption (dashed line) isotherms at 298 K for Fe-MOF@COF and the physical mixture for comparison.

hydrophobicity of these materials and highlighted the composite's capability to adsorb aromatic molecules at its interface, underscoring its potential as a promising material for organic pollutant removal in water treatment applications.

Dual properties for the degradation of bisphenol-A

In terms of applicability, the use of Fe-MOF@COF addresses the limitations associated with the impracticality of employing MOF powders in continuous-flow chemistry. This is primarily due to the tendency of TAPB–BTCA-COF to form aggregates rather than small individual particles, which facilitates the creation of a fixed bed. In this work, a chromatography column was packed with the composite for the capture and catalytic reaction of BPA under continuous flow conditions (Scheme 1). An aqueous solution of BPA (50 mg L^{-1}) and H_2O_2 (160 equivalents) was pumped through the column (20 mg of material packed, 6.3 mol% Fe) at a flow rate of 0.2 mL min^{-1} and 60 °C. The outlet solution was periodically monitored by measuring the UV-Visible absorption at 279 nm.

The process achieved an average BPA removal yield of 77% over 2 hours. A comparison between the capture-only process (in the absence of H_2O_2) and the dual process involving both capture and degradation (in the presence of H_2O_2) provides valuable insights (Fig. 6). The capture process proceeds rapidly at first, reflecting the strong affinity of TAPB–BTCA-COF for BPA; however, its efficiency declines over time due to progressive pore saturation. In contrast, the dual process sustains higher removal yields, as the degradation step helps regenerate active sites and delays their saturation. This behaviour suggests that a steady state is reached after approximately 40 minutes, in which both capture and degradation processes coexist, as indicated by the red line in Fig. 6. This degradation profile was obtained by subtracting the contribution of the capture-only process from the overall BPA removal. It is worth noting that the composite captures BPA through π–π interactions, but does not effectively capture phenol (see Fig. S14.1 from SI), a benchmark degradation product. The more hydrophilic degradation products detach from the surface of the composite, releasing the active adsorption sites and undergoing further mineralization (see S14 from SI).

Higher BPA concentrations resulted in saturation of the catalytically active sites, leading only to adsorption without observable degradation. Under those conditions, the dual functionality of the material—simultaneous capture and catalytic degradation—could not be achieved. Importantly, the effective performance of the composite at low BPA concentrations is particularly relevant for realistic water treatment scenarios, where pollutants are typically present at trace levels.

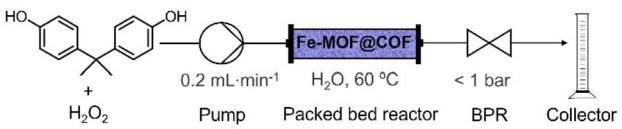

Scheme 1 Continuous Fenton reaction and capture of BPA.

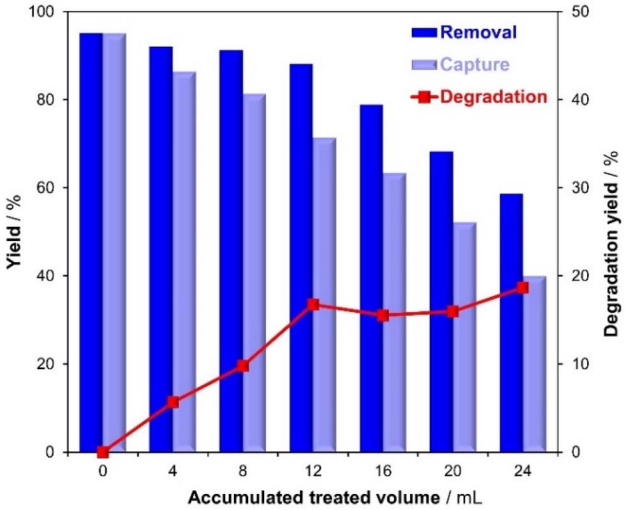

Fig. 6 Removal of BPA under flow conditions using Fe-MOF@COF, highlighting the capture and degradation processes.

Furthermore, the implementation of the physical mixture proved impractical mainly due to overpressure in the system, which exceeded 2 bars during the process. This approach also resulted in lower reaction rates and significantly higher leaching of iron and zirconium (see S14 from SI), highlighting the need for composites in terms of stability and enhanced mechanical properties. Additional results from various studies, including batch removal tests and experiments with alternative fillers such as the COF and the composite without iron, confirm that only the Fe-MOF@COF demonstrated this dual capture and catalytic activity. With a removal efficiency of 77%, this composite exhibited the highest performance among all tested materials (see Fig. S14.7 from SI), underscoring its unique ability to degrade and capture the pollutant simultaneously. Additionally, a comprehensive literature review was conducted to compare the activity of our system with that of other COF and MOF hybrids (see Table S14.3 from SI).

Moreover, the Fe-MOF@COF material was treated with ethanol and dried overnight after catalysis, and subsequently characterized using various techniques (XRD, FTIR, ICP, XAS, and PDF; see Fig. S14 in the SI). The results confirmed that the structure remained well-preserved, with low leaching rates of iron and zirconium (7% and 2% per h, respectively), thus demonstrating the stability and durability of the composite catalyst under continuous-flow conditions.

Conclusions

In conclusion, a novel Fe-MOF@COF composite material has been developed for water remediation applications and synthesized *via* a sustainable and mild sonochemical approach. Advanced synchrotron characterisation techniques, including PDF analysis, were employed to elucidate the interfacial interactions within the hybrid composite. Notably, the nature of the porous interface, enriched with π–π stacking interactions and hydrogen bonding between the MOF and COF backbones, was

identified, providing valuable structural insights. The Fe-MOF@COF composite demonstrated significant potential in continuous flow water decontamination, effectively capturing and degrading BPA. This dual functionality, combining adsorption and catalytic degradation, offers a promising solution for water purification. Moreover, both the high stability and minimal iron leaching observed after catalysis highlight the material's durability for long-term applications. This work opens new avenues for the design and characterisation of MOF@COF composites that simultaneously address adsorption and catalytic degradation for environmental applications.

Conflicts of interest

There are no conflicts to declare.

Data availability

The data supporting this article have been included as part of the SI. See DOI: https://doi.org/10.1039/d5ta03279b.

Acknowledgements

This work was supported by the grants PID2021-123839OB-I00, PID2022-138908NB-C31, RYC2018-024328-I and CNS2022-135261 funded by MICIU/AEI/10.13039/501100011033, and the NextGenerationEU/PRTR. A. E. P.-P. and F. Z. acknowledge the financial support from the Spanish Ministry of Science and Innovation, through the "María de Maeztu" Programme for Units of Excellence in R&D (CEX2018-000805-M & CEX2023-001316-M). C. M. acknowledges the financial support of the Madrid Government under the Multiannual Agreement with Universidad Autónoma de Madrid in the context of the V PRICIT (SI1/PJI/2019-00505). I. C.-V. acknowledges FPI-UAM 2021 fellowship UAM. C. C. B. and T. D. B. thank the Leverhulme Trust for a Research Project Grant (RPG-2020-005) and the Royal Society for a research grant (RSG\R1\180395). F. Z. acknowledges the support from the "(MAD2D-CM)-UAM" project funded by Comunidad de Madrid, by the Recovery, Transformation and Resilience Plan, and by NextGenerationEU from the European Union and wish to thank Comunidad de Madrid for the financial support to the CMOFs4water-CM Project (TEC-2024/ECO-332) through the R&D activities programme "Tecnologías2024". The authors want to thank Diamond Light Source for beamtime (proposal CY34797-1), and I15-1 staff for their assistance, as well as for beamtime (proposal SP35948-1), and B18 staff for their assistance.

Notes and references

1 H.-C. Zhou and S. Kitagawa, *Chem. Soc. Rev.*, 2014, **43**, 5415–5418.
2 C. S. Diercks and O. M. Yaghi, *Science*, 2017, **355**, aal1585.
3 H. D. Lawson, S. Patrick Walton and C. Chan, *ACS Appl. Mater. Interfaces*, 2021, **13**, 7004–7020.
4 S. Rojas and P. Horcajada, *Chem. Rev.*, 2020, **120**, 8378–8415.
5 C. Arqueros, F. Zamora and C. Montoro, *Nanomaterials*, 2021, **11**, 1651.
6 O. F. Altundal, C. Altintas and S. Keskin, *J. Mater. Chem. A*, 2020, **8**, 14609.
7 M. Rubio-Martinez, C. Avci-Camur and A. W. Thornton, *Chem. Soc. Rev.*, 2017, **46**, 3453.
8 M. S. Lohse, T. Bein, M. S. Lohse and T. Bein, *Adv. Funct. Mater.*, 2018, **28**, 1705553.
9 Z. Chen, X. Li, C. Yang, K. Cheng, T. Tan, Y. Lv and Y. Liu, *Adv. Sci.*, 2021, **8**, 2101883.
10 S. W. Lv, J. M. Liu, C. Y. Li, N. Zhao, Z. H. Wang and S. Wang, *Chemosphere*, 2020, **243**, 125378.
11 F. Ahmadijokani, A. Ghaffarkhah, H. Molavi, S. Dutta, Y. Lu, S. Wuttke, M. Kamkar, O. J. Rojas and M. Arjmand, *Adv. Funct. Mater.*, 2024, **34**, 2305527.
12 S. Liu, H. Li, Y. Shuai, Z. Ding and Y. Liu, *Mater. Adv.*, 2022, **3**, 8647.
13 M. L. Gao, M. H. Qi, L. Liu and Z. B. Han, *Chem. Commun.*, 2019, **55**, 6377.
14 X. Luo, C. Wang, G. Huang, Y. Tan, W. Tang, J. Kong and Z. Li, *Sep. Purif. Technol.*, 2022, **298**, 121616.
15 H. Y. Zhang, Y. Yang, C. C. Li, H. L. Tang, F. M. Zhang, G. L. Zhang and H. Yan, *J. Mater. Chem. A*, 2021, **9**, 16743.
16 C. Castillo-Blas, A. M. Chester, R. P. Cosquer, A. F. Sapnik, L. Corti, R. Sajzew, B. Poletto-Rodrigues, G. P. Robertson, D. J. M. Irving, L. N. McHugh, L. Wondraczek, F. Blanc, D. A. Keen and T. D. Bennett, *J. Am. Chem. Soc.*, 2023, **145**, 22913–22924.
17 I. del Castillo-Velilla, A. Sousaraei, I. Romero-Muñiz, C. Castillo-Blas, A. S. J. Méndez, F. E. Oropeza, V. A. de la Peña O'Shea, J. Cabanillas-González, A. Mavrandonakis and A. E. Platero-Prats, *Nat. Commun.*, 2023, **14**, 2506.
18 I. del Castillo-Velilla, I. Romero-Muñiz, C. Marini, C. Montoro and A. E. Platero-Prats, *Nanoscale*, 2024, **16**, 6627.
19 C. Castillo-Blas, I. Romero-Muñiz, A. Mavrandonakis, L. Simonelli and A. E. Platero-Prats, *Chem. Commun.*, 2020, **56**, 15615.
20 I. Romero-Muñiz, A. Mavrandonakis, P. Albacete, A. Vega, V. Briois, F. Zamora and A. E. Platero-Prats, *Angew. Chem., Int. Ed.*, 2020, **59**, 13013–13020.
21 X. Zhong, Z. Lu, W. Liang and B. Hu, *J. Hazard. Mater.*, 2020, **393**, 122353.
22 Y. Li, C. X. Yang and X. P. Yan, *Chem. Commun.*, 2017, **53**, 2511.
23 B. Bueken, N. Van Velthoven, T. Willhammar, T. Stassin, I. Stassen, D. A. Keen, G. V. Baron, J. F. M. Denayer, R. Ameloot, S. Bals, D. De Vos and T. D. Bennett, *Chem. Sci.*, 2017, **8**, 3939.
24 W. Zhao, P. Yan, B. Li, M. Bahri, L. Liu, X. Zhou, R. Clowes, N. D. Browning, Y. Wu, J. W. Ward and A. I. Cooper, *J. Am. Chem. Soc.*, 2022, **144**, 9902–9909.
25 W. Zhao, P. Yan, H. Yang, M. Bahri, A. M. James, H. Chen, L. Liu, B. Li, Z. Pang, R. Clowes, N. D. Browning, J. W. Ward, Y. Wu and A. I. Cooper, *Nat. Synth.*, 2022, **1**, 87–95.

26 T. E. Westre, P. Kennepohl, J. G. Dewitt, B. Hedman, K. O. Hodgson and E. I. Solomon, *J. Am. Chem. Soc.*, 1997, **119**, 6297–6314.
27 L. Garzón-Tovar, J. Pérez-Carvajal, A. Yazdi, J. Hernández-Muñoz, P. Tarazona, I. Imaz, F. Zamora and D. Maspoch, *Angew. Chem., Int. Ed.*, 2019, **131**, 9612–9616.
28 C. Castillo-Blas, J. M. Moreno, I. Romero-Muñiz and A. E. Platero-Prats, *Nanoscale*, 2020, **12**, 15577.
29 I. Romero-Muñiz, E. Loukopoulos, Y. Xiong, F. Zamora and A. E. Platero-Prats, *Chem. Soc. Rev.*, 2024, **53**, 11772–11803.
30 A. M. Chester, C. Castillo-Blas, R. Sajzew, B. P. Rodrigues, R. Mas-Balleste, A. Moya, J. E. Snelson, S. M. Collins, A. F. Sapnik, G. P. Robertson, D. J. M. Irving, L. Wondraczek, D. A. Keen and T. D. Bennett, *Chem. Sci.*, 2023, **14**, 11737.
31 V. Nozari, A. N. V. Azar, R. Sajzew, C. Castillo-Blas, A. Kono, M. Oschatz, D. A. Keen, P. A. Chater, G. P. Robertson, J. M. A. Steele, L. León-Alcaide, A. Knebel, C. W. Ashling, T. D. Bennett and L. Wondraczek, *Small*, 2024, **20**, 2303315.
32 L. S. Xie, E. V. Alexandrov, G. Skorupskii, D. M. Proserpio and M. Dincă, *Chem. Sci.*, 2019, **10**, 8558.